J. Phys. Chem. B **2010,** *114,* 6089–6098

Dielectric Constant of Ice Ih and Ice V: A Computer Simulation Study

Luis G. MacDowell* and Carlos Vega

Departamento de Química Física, Facultad de Ciencias Químicas, Universidad Complutense de Madrid, 28040, Spain

Received: January 7, 2010; Revised Manuscript Received: March 18, 2010

In this work, we exploit an efficient algorithm for the sampling of hydrogen-bond networks in order to study the order/disorder transition and the dielectric properties of ice Ih. Our results show that all of the rigid point charge models studied, TIP4P/Ice, TIP4P/2005, TIP4P, and SPC/E, yield a very low dielectric constant as compared with experiment. The analysis of the polarization factor, G, reveals that the structure of ice Ih as predicted by the TIP4P family of models studied is very similar. For all such models, $G \approx 2.5$, the differences in the dielectric constant being given mainly by the different molecular dipole moments. The angular correlations in the SPC/E model are very different, however, yielding $G \approx 1.8$. Our study suggests that the dielectric anisotropy of ice Ih is very small and at any rate smaller than the statistical uncertainty of our results. We show that for sufficiently anisotropic structures, such as ice V, the method employed does indeed reveal a strong anisotropy. At 5000 bar and 180 K, we find that the principal dielectric constants of ice V according to the TIP4P/Ice model are 34, 164, and 76. The order/disorder transition could not be well characterized, because of very strong hysteresis. Whereas low temperature ordered phases were readily disordered at temperatures below 50 K, the high temperature phase remained disordered upon cooling. Nevertheless, our plots of dielectric constant versus temperature reveal a clear lambda-like shape and obey a Curie−Weiss law. All of the models studied show a higher stability of the antiferroelectric $Pna2_1$ phase than the experimental ferroelectric $Cmc2_1$ phase.

Introduction

Ordinary ice, also known as ice Ih is not quite an ordinary crystal. Rather, oxygen atoms lay on regular lattice positions forming hexagonal rings, but the hydrogen positions may be chosen such that water molecules adopt randomly one out of six possible orientations.[1] Ice Ih is therefore a rotational disordered crystal, although the number of possible configurations that contribute are limited to those obeying the Bernal−Fowler rules. Consistent with the tetrahedral arrangement of hydrogen bonds which is also found to a smaller extent in liquid water, the possible realizations of the lattice are separated by large energy barriers, of the order of two hydrogen bonds, and hence, the sampling of molecular orientations within the crystal is very slow. It is widely believed that such sampling requires collective rearrangements involving cooperative rotation of at least six water molecules along a ring. Such a slow dynamics points to dielectric relaxation as the most appropriate technique for probing the orientation rearrangements. Johari and Whalley have estimated that the relaxation time of such modes is several microseconds at the melting temperature but may become many years long at 100 K. In practice, however, the presence of impurities lowers the free energy for creation of rotational defects and provides an extra path for relaxation below ca. $T =$ 240 K, though the time scales for relaxation remain well beyond the μs.[2]

As a result of this very slow dynamics, ice Ih displays a well-known violation of the third law. Cooling down to very low temperatures does not lead to any visible phase transition into a fully ordered phase. The system gets kinetically trapped into a rotational glass with a measurable entropy excess[3] that was first estimated by Pauling.[4] So far, this situation has only been remedied by doping ice with KOH. The doped sample so prepared then undergoes a phase transition into an orthorhombic ordered phase at about 70 K.[5−7] There are two possible orthorhombic ordered crystal structures compatible with a fixed orientation of the oxygens (cf., Figure 1). One is an antiferroelectric phase with space group $Pna2_1$ (A/$Pna2_1$) that was proposed theoretically by Davidson and Morokuma.[8] The other is a ferroelectric phase with space group $Cmc2_1$ (F/$Cmc2_1$) that was conjectured by Kamb and Minagawa.[9,10] All subsequent neutron diffraction studies on deuterated samples have favored the F/$Cmc2_1$ structure as the low temperature phase of ice.[11−14]

It does not come as a surprise that the computer simulation of ice might become a very tricky issue.[15] Sampling of the slow collective ring rotations by molecular dynamics is obviously out of question, but conventional Monte Carlo simulations are also unable to sample the possible hydrogen-bond networks consistent with the Bernal−Fowler rules. In practice, simulations are usually performed by choosing one possible realization of the hydrogen-bond network. Properties such as density or pressure are not much affected by the lack of sampling, while others such as the crystal's free energy may be corrected for the quenched disorder using Pauling's result for the residual entropy.[4]

Such tricks do not allow one to observe (directly) the order/disorder transition or low frequency dielectric properties. As a result, only a very limited number of simulation studies have been performed on the dielectric constant of ice. The first few were performed on a lattice and employed a Monte Carlo sampling technique that attempts to rotate cooperatively all of the molecules inside a ring.[16−18] Subsequently, Rick and Haymet extended this algorithm to off-lattice models.[19,20] More recently, Lindberg and Wang have proposed a different methodology

---

* To whom correspondence should be addressed. E-mail: luis@ender.quim.ucm.es.

10.1021/jp100167y

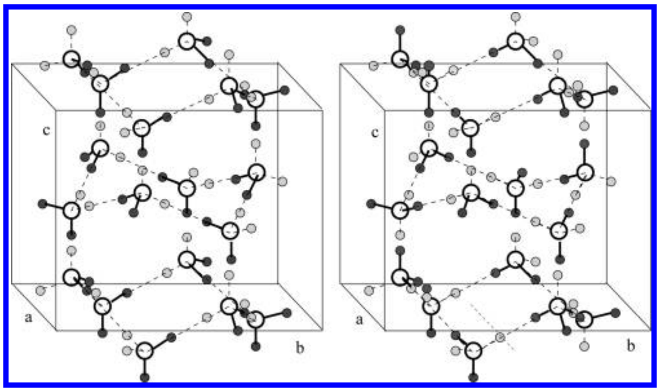

Figure 1. Possible orthorhombic structures for the low temperature−low pressure ordered phase of ice. Left, ferroelectric $Cmc2_1$ phase as determined experimentally (the upper and lower rings are obtained upon rotation about the screw 2_1 axis parallel to c and crossing $x = 1/2$, $b = 1/2$). Right, antiferroelectric $A/Pna2_1$ phase conjectured by Morokuma (the upper and lower rings are obtained from the central one upon reflection of a glide plane crossing the b axis at $b = 1/2$). In order to allow for comparison, the antiferroelectric phase is shown here under the nonstandard space group $P2_1cn$. The standard space group is obtained by interchanging the a and c axis and displacing the origin by 1/4 along the direction of the b axis. Hatched circles indicate fully occupied proton sites. In the high temperature phase, both the hatched and empty circles (unoccupied proton sites in the low temperature phase) adopt occupancies of 1/2. Under the convention followed in the figure, the extra symmetry leads to the nonstandard orthorhombic space group Cmc. This is equivalent to the standard $P6_3/mmc$ hexagonal phase of ice Ih.

which attempts to create a number of uncorrelated configurations by switching the electrostatic interactions smoothly from a fully spherical reference system.[21]

The availability of a technique that allows one to sample ring rotations may allow one to study ice more accurately than hitherto. In ice Ih, for example, the disorder is thought to be complete within a large temperature interval. A single representative realization of disorder may be used to sample many properties (with the notable exception of the dielectric constant). Furthermore, the Pauling entropy estimate that is added ad-hoc in free energy calculations has been found to be very close to the exact result estimated recently.[22,23] However, other solid phases of water, such as ice III and ice V exhibit partial disorder, and the amount of disorder changes continuously with temperature.[24,25] This problem can be somewhat remedied by preparing partially disordered configurations that are compatible with experimental findings, as described in ref 26. Unfortunately, such configurations need not be fully consistent with the force field employed, and usual Monte Carlo techniques will not allow for changes in the hydrogen-bond network with temperature.

In this work, we employ the ring rotation method proposed by Rick and Haymet,[19] in order to study the spontaneous disordering of initial ordered structures, as well as to calculate the dielectric properties of ice. We will consider two well-known water models, TIP4P and SPC/E,[27,28] as well as two other recently developed models, TIP4P/Ice and TIP4P/2005.[29,30] The last two models provide a significant improvement over TIP4P and yield also good results for more complex systems.[31−33] By using this technique, we are able to observe ring excitations, follow the temperature dependence of the hydrogen-bond network, and accurately measure the dielectric constant.

The remaining of the paper is arranged as follows. In the next section, we present the theoretical framework needed to calculate the dielectric constant with due account of the anisotropy. The next section describes the method that has been employed to properly sample the hydrogen-bond network. Subsequently, a section is devoted to gather all the results and finally the main conclusions of this work are presented.

Theory

The relation of the dielectric constant with molecular properties has been a subject of much debate.[34] It was not until Kirkwood and Fröhlich that a clear relation could be established.[35,36] However, with the advent of computer simulations, the standard result needed generalization in order to properly account for the assumed boundary conditions, and this also required careful reexamination of the problem.[37−39] Whereas the working expressions for isotropic materials are now well established,[40,41] the calculation of dielectric constants of anisotropic materials from molecular considerations has been seldom considered.[9,19,37,42] A brief summary of the working equations is presented here.

The average dipole moment of a dielectric material under the effect of an external field $\mathbf{E_e}$ is given by

$$\langle \mathbf{M}\rangle_{\mathbf{E_e}} = \int \mathbf{M} e^{-\beta[U-\mathbf{M}\cdot\mathbf{E_e}]}\,d\Gamma / \int e^{-\beta[U-\mathbf{M}\cdot\mathbf{E_e}]}\,d\Gamma \qquad (1)$$

where $\mathbf{M}$ is the instantaneous dipole moment, U is the potential energy in the absence of a field, and $d\Gamma$ denotes integration over configuration space. Expanding this equation to first order in the field, we find

$$\langle \mathbf{M}\rangle_{\mathbf{E_e}} = \langle \mathbf{M}\rangle_0 + \beta\langle \mathbf{M}\mathbf{M}\cdot\mathbf{E_e}\rangle_0 - \beta\langle \mathbf{M}\rangle_0\langle \mathbf{M}\cdot\mathbf{E_e}\rangle_0 \qquad (2)$$

For a dielectric material, we expect $\langle \mathbf{M}\rangle_0$ to vanish. However, in the course of a simulation, where the sampling is limited to part of configuration space, or in a ferroelectric material, we may find a net polar moment. We will therefore retain this term for the time being. The average polarization due to the field can then be written as

$$\Delta\mathbf{P} = \frac{\beta}{V}[\langle \mathbf{M}\mathbf{M}\rangle_0 - \langle \mathbf{M}\rangle_0\langle \mathbf{M}\rangle_0]\cdot\mathbf{E_e} \qquad (3)$$

where $\Delta\mathbf{P} = \mathbf{P}_{\mathbf{E_e}} - \mathbf{P}_0$, $\mathbf{P}$ is the dipole moment per unit volume or polarization and the notation $\mathbf{AB}$ denotes a dyad with matrix elements $AB_{\alpha\beta} = A_\alpha B_\beta$. For an isotropic dielectric, the term in squared brackets may be written as a diagonal matrix, because the polarization is always parallel to the applied field. For an anisotropic material, however, this is not generally the case and tensor notation must be retained.

The averaged macroscopic field within the dielectric medium includes the effect of the external field as well as that created by the material's polarization. At the macroscopic scale, the polarization is uniform and we can write

$$\mathbf{E} = \mathbf{E_e} + \mathbf{T}_\mathrm{m}\cdot\mathbf{P} \qquad (4)$$

where $\mathbf{T}_\mathrm{m}$ is the volume integral of the dipole−dipole tensor and the subscript recalls this has to be suitably modified to account for the chosen boundary conditions of the simulation.[39] In accordance with the preceding microscopic description, we account explicitly for the presence of a net polarization of the sample within the limited time of observation, so that the above equation is written as

$$\mathbf{E} = \mathbf{E_e} + \mathbf{T}_m \cdot \mathbf{P}_0 + \mathbf{T}_m \cdot \Delta\mathbf{P} \tag{5}$$

The second term of the right-hand side can be immediately identified with the microscopic field, $\mathbf{E}_0$, created by the material in the absence of an external field. We can therefore write

$$\Delta\mathbf{E} = \mathbf{E_e} + \mathbf{T}_m \cdot \Delta\mathbf{P} \tag{6}$$

where $\Delta\mathbf{E} = \mathbf{E} - \mathbf{E}_0$.

In order to relate this equation with eq 3, we need to supplement the macroscopic description with a constitutive equation relating the field with the polarization. Comparing eq 6 with eq 3, it becomes apparent that $\Delta\mathbf{P}$ must be linearly related to $\Delta\mathbf{E}$, so that we must accept the following modified constitutive relation:

$$\Delta\mathbf{P} = \chi \cdot \Delta\mathbf{E} \tag{7}$$

where χ is the susceptibility tensor of the dielectric material. Whereas this is somewhat unusual for the definition of the electric susceptibility, it is the implied constitutive relation employed usually in simulations.[19,21,41]

Substitution of the constitutive relation into eq 6 yields

$$[\chi^{-1} - \mathbf{T}_m] \cdot \Delta\mathbf{P} = \mathbf{E_e} \tag{8}$$

Further substitution of eq 3 into the above result yields[37]

$$\left\{\frac{\beta}{V}[\chi^{-1} - \mathbf{T}_m] \cdot [\langle\mathbf{MM}\rangle_0 - \langle\mathbf{M}\rangle_0\langle\mathbf{M}\rangle_0] - \mathbf{I}\right\} \cdot \mathbf{E_e} = \mathbf{0} \tag{9}$$

Since this equation must hold for arbitrary external fields, it is clear that the term in curly brackets must vanish for the equality to hold. It follows that the susceptibility tensor is the solution of the following linear equation:

$$\chi\left[\mathbf{T}_m + \frac{V}{\beta}\mathbf{F}^{-1}\right] = \mathbf{I} \tag{10}$$

where $\mathbf{I}$ is the unit matrix and $\mathbf{F}$ is the dipole moment fluctuation tensor:

$$\mathbf{F} = \langle\mathbf{MM}\rangle_0 - \langle\mathbf{M}\rangle_0\langle\mathbf{M}\rangle_0 \tag{11}$$

Equation 10 is the general solution for the susceptibility tensor of an anisotropic dielectric material. The solution depends formally on the assumed boundary conditions, which are explicitly accounted for in the integrated modified dipole–dipole tensor, $\mathbf{T}_m$. In computer experiments, it has been convenient to assume a spherical sample of dielectric material surrounded by an isotropic dielectric.[40,41] In such a case,[38]

$$\mathbf{T}_m = -\frac{4\pi}{2\varepsilon_s + 1}\delta_{\alpha\beta} \tag{12}$$

where ε_s is the dielectric constant of the surrounding medium. Several choices for the surrounding medium have been studied.[43,44] One simple such choice is to consider the material surrounded by a vacuum, as in the Lorentz–Lorenz theory. Another possible choice is to assume surroundings of the same material as the sample employed (similar to the Kirkwood–Frohlich theory). However, this choice requires a priori knowledge of the dielectric constant. The situation is further complicated if the surrounding material is anisotropic, as not only the principal dielectric constants are required *a priori* but also the principal dielectric axes.[42] Hence, in most practical situations, one chooses conducting boundary conditions, so that $\varepsilon_s = \infty$ and $\mathbf{T}_m$ may be ignored altogether. The general solution then takes the simple form

$$\chi = \frac{\beta}{V}\mathbf{F} \tag{13}$$

For an isotropic medium (such as cubic crystals), a properly averaged $\mathbf{F}$ tensor should become diagonal for whatever choice of reference frame, all the diagonal elements are equal, and the equation may be solved right away for the dielectric constant by performing the trace operation on both sides of the equation. For anisotropic materials, $\mathbf{F}$ will not generally be diagonal. However, there exists a coordinate system fixed in the crystal such that $\mathbf{F}$ is diagonal. Furthermore, the orientation of the principal dielectric axes is given by symmetry in most crystal structures (trigonal, tetragonal, hexagonal, and orthorhombic), the principal axes not being trivial relative to the crystallographic axis only for monoclinic and triclinic structures.[45] At any rate, for conducting boundary conditions, the problem of finding the principal dielectric constants and axes is reduced to suitable diagonalization of $\mathbf{F}$, such that

$$\frac{\varepsilon_{\alpha\beta} - 1}{4\pi}\delta_{\alpha\beta} = \frac{\langle M_\alpha M_\beta\rangle_0 - \langle M_\alpha\rangle_0\langle M_\beta\rangle_0}{k_B T V}\delta_{\alpha\beta} \tag{14}$$

Note that this equation accounts explicitly for a nonvanishing polarization in analogy with results for isotropic media.[40,41] Whereas an ordinary dielectric has vanishing polar moment at zero field, the subtraction of the squared average polarization of the simulation could remedy for bad sampling. Alternatively, one could assume this result as a generalization to ferroelectric materials. The electric response of ferroelectric materials is highly nonlinear and known to exhibit a characteristic hysteresis loop.[34] However, we expect that eq 14 may be employed in order to describe the linear response of the material after attainment of the remanent polarization. On the other hand, application of eq 14 with an assumed zero polarity could account for the dielectric response of a multidomain crystal with zero net polarization. Nevertheless, we stress that the result of eq 14 is consistent with the modified constitutive relation, eq 7. Obviously, this equation is fully consistent with the more usual $\mathbf{P} = \chi \cdot \mathbf{E}$ for the case of vanishing average polarization at zero field.

Simulations

Monte Carlo simulations were carried out in the NpT ensemble.[40] Typically, we employed an arrangement of 5 × 3 × 3 orthorhombic unit cells with a total of 360 molecules, though some simulations were carried out with $N = 128$ molecules. Box deformations were dealt with using the Parrinello–Rahman method.[46] Coulombic interactions were calculated using the Ewald summation technique.[37] Conducting boundary conditions were employed in all simulations. Both

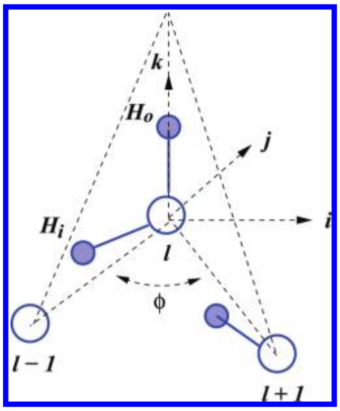

Figure 2. Schematic representation of the loop rotation algorithm by Rick and Haymet.[19] H_i which is a proton donor in the loop containing oxygens $l-1$, l, and $l+1$ is rotated about vector $\mathbf{k}$ by an amount equal to the dihedral angle between planes $H_0{-}O_l{-}O_{l-1}$ and $H_0{-}O_l{-}O_{l+1}$ (see text). In this way, the bond $O_l{-}H_i$, initially lying close to the plane $H_0{-}O_l{-}O_{l-1}$, now lies close to the $H_0{-}O_l{-}O_{l+1}$ plane.

dispersive and screened-Coulombic interactions up to the cutoff distance were calculated by means of an efficient link cell list.[47] Usual long-range corrections for the Lennard-Jones interactions were added and the pair potential was truncated at 8.5 Å for all models.[40]

It is well-known that a standard Metropolis algorithm incorporating only displacement and rotation attempts cannot properly sample ice. These movements will sample small amplitude vibrations and librations but are unable to modify the assumed hydrogen-bond arrangements within a reasonable amount of CPU time. An algorithm for exploring hydrogen-bond arrangements was proposed by Rahman and Stillinger for a simple tetrahedral lattice model.[48] This algorithm was also exploited later on to study the order/disorder transition of ice on a lattice,[17,18] and was extended recently for off lattice water models.[19] The method requires one first to search for a closed loop of hydrogen bonds. Molecules belonging to the loop have one proton that is a bond donor inside the loop (inner bond) and another that is not (outer bond). The attempted move consists of successive rotation of the molecules about their outer bond by 120° until a full hydrogen-bond arrangement with opposite sense has been established along the loop. The attempted move is accepted or rejected according to the usual Monte Carlo lottery. Whereas this algorithm works well for tetrahedral lattices, the acceptance may become too low in off lattice systems. Rick and Haymet have argued that a greater acceptance is achieved rotating the molecule by the dihedral angle formed between planes $H_0{-}O_l{-}O_{l-1}$ and $H_0{-}O_l{-}O_{l+1}$ (see Figure 2). In this way, the angle of rotation is accommodated to the instantaneous distorted geometry of the lattice. The algorithm is further sped up by creating a list of hydrogen-bond donors and acceptors for each molecule at the beginning of the simulation. The list is then used to avoid calculating nearest neighbors and bond donors/acceptors during the loop search and updated each time a loop rotation is accepted.

The topology of loops in a crystal was studied by Rahman and Stillinger.[48] They found that rings could be classified into three classes: (i) true closed loops with six molecules, (ii) true closed loops with more than six molecules, and (iii) percolating loops, which span one full linear dimension of the simulation box and are closed by virtue of the periodic boundary conditions. By performing a Markov chain over loop rotations, all of the hydrogen-bond arrangements may be sampled in principle. However, acceptance of loop rotations is highly dependent on loop size, and this may become a problem. For ice Ih, with full proton disorder, Rahman and Stillinger observed that the overwhelming majority of rings have six bonds. Such rings have a small but significant acceptance rate, so that a good sampling may be achieved for the disordered phase. Unfortunately, the transition between ordered and disordered phases will usually require sampling large percolating rings, which have a very low acceptance. For this reason, the algorithm runs into trouble close to phase transitions, and more so for large system sizes which require rotation of large percolating rings. That the sampling of order/disorder transitions may become difficult may be easily illustrated by considering a perfect tetrahedral lattice. In such cases, it is easy to show that full rotation of a closed loop leaves the total dipole moment unchanged.[17] However, the disordered Ih phase of ice has no net dipole moment on average, while the ordered $Cmc2_1$ phase of ice is ferroelectric. Hence, transition from one to the other requires rotation of a percolating loop.

The simulations were organized in batches. First, a series of simulations were started from the low temperature ordered phase at either 5 or 10 K, and heated gradually along a *heating batch*. Each production stage along the batch consisted of 200 thousand cycles following a previous equilibration stage of 50−100 thousand cycles. Subsequent *cooling batches* starting from high temperature configurations were also performed in order to study hysteresis effects. Ordered phases beyond the disordering transition were studied by means of *frustrated heating batches* consisting of MC simulations with loop moves switched off (with translation and rotation in the ratio 50:50). The simulations within a batch consisted of several hundred thousand cycles each. A cycle comprises N trial translation, rotation or loop moves in the ratio 40:40:20, followed by one box deformation attempt. All simulations are performed at a pressure of 1 bar unless so stated.

Results

Test of Loop Moves. In order to obtain reliable dielectric constants, we first need to show that the loop rotation algorithm samples efficiently the hydrogen-bond network. This was tested by heating low temperature ordered configurations until full disorder was achieved.

To asses the extent of disordering, we first need to find an appropriate order parameter. Figure 3 shows a schematic representation of water molecules within the F/$Cmc2_1$ and A/$Pna2_1$ crystal structures. The Greek letters next to nonequivalent hydrogen sites denote the site occupancies. These are either 1 or 0 for the fully ordered phase and become 1/2 for the proton disordered ice Ih. Monitoring each of the three hydrogen site occupancies is awkward, so we devise an order parameter as a linear combination of α, β, and γ. For the F/$Cmc2_1$ phase, we define a ferroelectric order parameter as

$$O_F = \frac{2}{3}(2 + \gamma - \alpha - \beta) - 1 \qquad (15)$$

In the fully ordered phase, we have $\alpha = \beta = 0$ and $\gamma = 1$, so that $O_F = 1$. In the disordered phase, $\alpha = \beta = \gamma = 1/2$ so that O_F vanishes. For the antiferroelectric $Pna2_1$ phase, we define an antiferroelectric order parameter as

$$O_A = \frac{2}{3}(3 - \alpha - \beta - \gamma) - 1 \qquad (16)$$

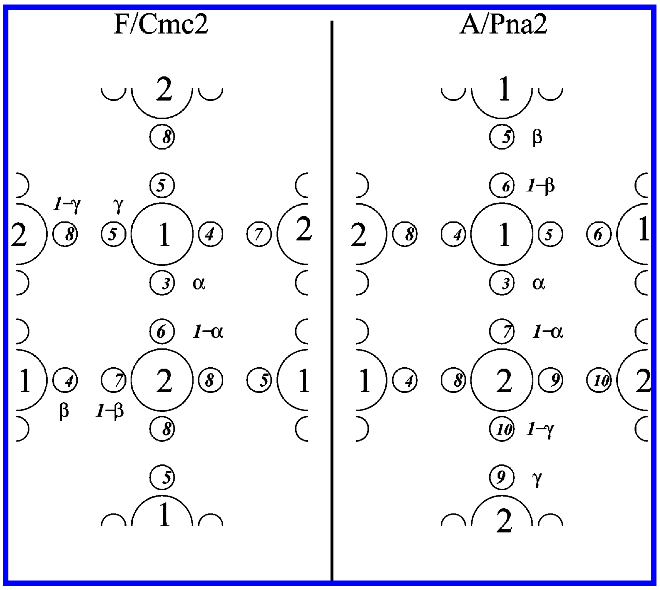

Figure 3. Local environment of the nonequivalent water molecules in ice XI. The large circles denote oxygen atoms, while the small circles denote possible hydrogen sites. The numbers indicate nonequivalent crystallographic sites, and the Greek letters stand for the corresponding hydrogen site occupancies.

Here, $\alpha = \beta = \gamma = 0$ in the ordered phase, so that $O_A = 1$. For the disordered phase, $\alpha = \beta = \gamma = 1/2$ and the order parameter becomes zero.

Figure 4 shows the order parameters of the TIP4P/Ice model obtained during the heating batch from 5 to 100 K for either the ferroelectric or antiferroelectric ordered phases as initial configurations. In both cases, the low temperature phases rapidly disorder as reflected by the vanishing value of the corresponding order parameter. Clearly, the loop rotation algorithm is able to efficiently disorder the initially ordered configurations even at temperatures as low as 10−20 K. This occurs despite the fact that, as mentioned earlier, the disordering requires rotation of large percolating loops of at least 10 (for the antiferroelectric phase) or 12 molecules (for the ferroelectric phase). Similar results were obtained for TIP4P/2005 and TIP4P models. The SPC/E model behaved quite differently, since neither of the ordered phases could disorder until about 200 K. This is most likely a problem of ergodicity, revealing large activation energies between different hydrogen-bond networks, since previous calculations suggest that the order/disorder transition of the SPC/E model lies between 43 and 84 K.[20,49]

Once the system is disordered, most of the loops are of hexagonal shape and comprise only six molecules.[48] Since the algorithm is able to rotate loops of at least 10 molecules at very low temperature, we expect it will properly sample 6 molecule loops at high temperature and hence properly explore the full hydrogen-bond network.

We note that the order parameters defined above only show the departure from the corresponding ordered phase but are not able to discriminate between different ordered phases; i.e., the A/*Pna*2$_1$ phase described within the F/*Cmc*2$_1$ space group will provide $O_F = 0$, just as the disordered phase. Similarly, the F/*Cmc*2$_1$ phase described within the A/*Pna*2$_1$ space group will yield $O_A = 0$. In order to discriminate between the ferroelectric, antiferroelectric, or disordered phases in terms of occupation numbers would require describing the system with the common space group *Pc* of lower symmetry. This implies monitoring eight different occupation parameters, and was not attempted.

However, we can show further evidence that the initial configurations have disordered by looking at the (unweighted angle average of the) dielectric constants obtained during the heating batches, which we define as

$$\varepsilon = \frac{1}{3}Tr(\boldsymbol{\varepsilon}) \tag{17}$$

Figure 5 shows the results for TPT4P/Ice, where we find a λ-like curve typical of disordering transitions. Clearly, the dielectric constants from the two heating batches become equal at about 75 K, showing that the system has completely lost memory of the initial configurations (note that at low temperature the ordered phases have very low dielectric constants of little more than unity and also look equal within the scale of the figure). Together with the heating batches, Figure 5 shows results for a cooling batch starting from the high temperature phase. It is interesting to note that the results also resemble a λ curve and suggest a moderately reversible transition. However, Figure 4 reveals that the phase transition, if any, has a strong hysteresis and the system is unable to rearrange during cooling. The state obtained while quenching is very much like a rotational glass.

Dielectric Constant. The previous tests give us confidence in the results obtained for the dielectric constant of the high temperature phase (Ice Ih) above about 100 K. As a further

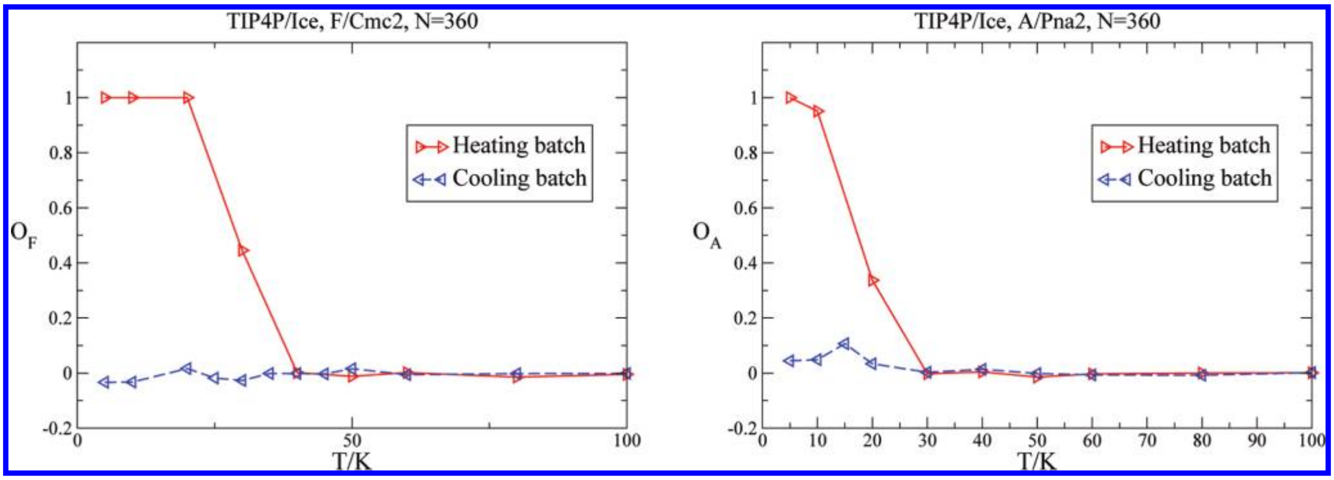

Figure 4. Ferroelectric (O_F) and antiferroelectric (O_A) order parameters during heating and cooling for the TIP4P/Ice model at 1 bar. Left, results for simulations starting from F/*Cmc*2$_1$. Right, results for simulations starting from A/*Pna*2$_1$. Triangles to the right indicate heating, while triangles to the left indicate cooling. The lines are a guide to the eye.

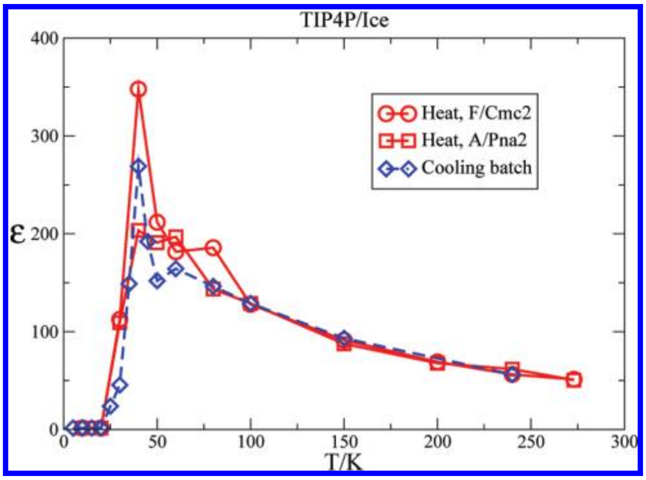

Figure 5. Dielectric constant for TIP4P/Ice at 1 bar. The circles correspond to a heating batch starting from F/*Cmc*2_1, while the squares are a similar heating batch from the A/*Pna*2_1 configuration. The diamonds are a cooling batch starting from the high temperature disordered phase.

check, our results for the TIP4P model yield very good agreement with previous results by Rick and Haymet,[19] and lie a few percent below those obtained by Lindberg and Wang.[21] Considering the scatter that is found in calculations of the dielectric constant of liquid water, these differences seem acceptable. Table 1 collects our results for ice Ih above $T =$ 150 K.

Figure 6 shows results obtained for the dielectric constant of ice Ih as a function of temperature for five different water models. Three models of the TIP4P family, namely, TIP4P/Ice, TIP4P/2005, and TIP4P, the SPC/E model, and the TIP5P model (as reported in ref 20). Results are compared with experimental results from Johari and Whalley for polycrystalline ice.[2] As noted previously for the TIP4P and SPC/E models,[19,21] the TIP4P/Ice and TIP4P/2005 models perform also very poorly as regards the dielectric constant of ice, yielding estimates that are about 40% lower than the experimental result. Furthermore, the dielectric constants that we find at $T = 273$ *K* are actually smaller than those obtained for the corresponding model in liquid water, a result at odds with experimental findings.[1] This trend is even more striking for the TIP5P model, which provides the dielectric constant of liquid water at ambient temperature in very good agreement with experiment but yields predictions that are far too small by a factor of 3 for ice at $T = 240$ K.

Despite the apparently smooth trend of the dielectric constant for these models, the angular correlations displayed differ considerably between the TIP4P and SPC/E models. This can be shown by studying the polarization tensor, which, consistent with eq 14, we define here as[40]

$$G_{\alpha\beta} = \frac{\langle M_\alpha M_\beta\rangle - \langle M_\alpha\rangle\langle M_\beta\rangle}{N{\mu_0}^2} \tag{18}$$

where μ_0 is the dipole moment of an individual water molecule in the medium. $G_{\alpha\beta}$ is a measure of the angular correlations due to molecular interactions. For an ideal gas, it takes the value of unity, and usually increases in disordered condensed phases. Note that **G** depends on the boundary conditions, so that, for ε_s equal to the dielectric constant of the sample, the trace of **G** becomes equal to Kirkwood's *g* factor.[40,51] Figure 7 shows the trace of the polarization tensor, $G = Tr(g_{\alpha\beta})$, for the models studied. All of the TIP4P models yield very similar results, with $G \approx 2.5$ almost constant from $T = 100$ K to beyond the melting temperature, while G is about 1.8 for the SPC/E model. We note that ice II is actually the stable phase of SPC/E water at normal pressure, with ice Ih being only metastable under these conditions.[15] We can nevertheless obtain an estimate for the dielectric constant because ice Ih is at least mechanically stable and can be simulated beyond its region of thermodynamic stability.[50] Clearly, the results point to weaker correlations in the SPC/E model. Experimentally, the product $G{\mu_0}^2$ may be calculated from Curie−Weiss plots of the dielectric constant.[2] Johari and Whalley found $G{\mu_0}^2$ almost constant above $T = 133$ K and about 26.4 D^2. Note that Johari and Whalley actually

TABLE 1: Dielectric Constant of Ice Ih above $T = 150$ K and $P = 1$ bar for Several Water Models

model	temperature 150	200	240	273
TIP4P/Ice	90(2)	70(1)	57(4)	51(1)
TIP4P/2005	83(2)	62(1)	53(1)	46(1)
TIP4P	75(2)	58(1)	47(1)	40(1)
TIP4P[a]	78(4)	57(3)	48(1)	
TIP4P[b]	84(1)	60(1)	51(1)	
SPC/E		49(5)	41(2)	
experimental[c]	174	130	108	95

[a] Results from Rick and Haymet. [b] Results from Lindberg and Wang. [c] Experimental results from Johari and Whalley.

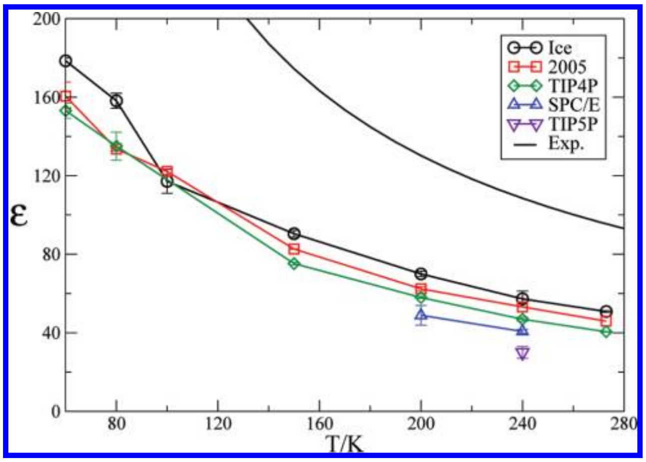

Figure 6. Dielectric constant at 1 bar for several water models (symbols) compared with a correlation (full line) of experimental results.[2] Results for TIP5P from ref 20.

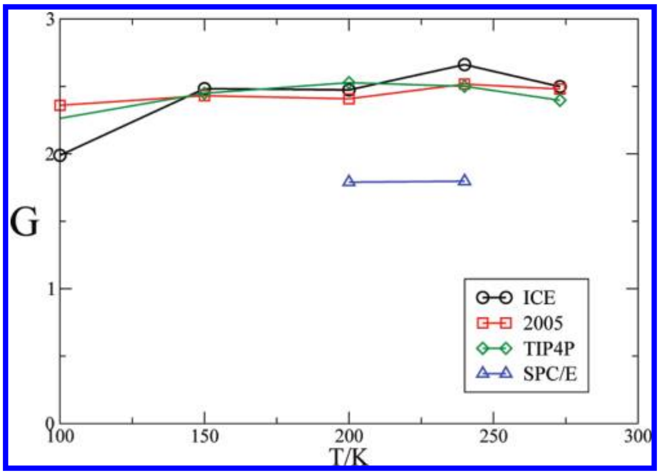

Figure 7. Polarization factor for several water models as obtained from heating batches.

report Kirkwood's g-factor, $g_k = 17.6$, which for high dielectric constants obeys $G/g_k = 3/2$.[51] Our results also predict $G\mu_0^2$ is close to constant but underestimate the experimental value considerably, as we obtain roughly 15, 13, 12, and 10 D^2 for the TIP4P/Ice, TIP4P/2005, TIP4P, and SPC/E models, respectively. This is not surprising, in view of estimates for the dipole of H_2O molecules in ice Ih, which is much higher than that of the models investigated here. Batista et al. used an induction model and estimated $\mu_0 = 3.09$ D.[52] More recently, Sharma et al. estimated with their quantum density functional calculations an effective net dipole moment at the melting temperature of about $\mu_0 = 3.32$ D.[53] In order to recover the experimental dielectric constant, $\varepsilon \approx 96.5$, this requires $G \approx 2.55$, in good agreement with predictions obtained from the TIP4P family.

The results obtained for ε correlate with the ratio of dipole to quadrupole moment, a property which was found previously to be important in describing the phase diagram of water models.[54,55] On the contrary, the dipole moment, which would appear to be the most relevant property determining the dielectric constant, does not quite correlate as good, since the moments of the models studied follow the trend TIP4P/Ice > SPC/E > TIP4/2005 > TIP4P. The reason is that, as noted previously, the quadrupole moment, Q_T, plays an important role too.[56] Large dipole moments do not always lead to a large increase of the dielectric constant, because orientation fluctuations may be strongly affected. Actually, large quadrupole moments strongly inhibit such fluctuations. From eqs 14 and 18, it would seem that the dependence of the angle averaged dielectric constant on μ_0 and Q_T may be written as

$$\varepsilon = 1 + \frac{4\pi\rho}{k_B T} G\left(\frac{\mu_0}{Q_T}\right)\mu_0^2 \tag{19}$$

Hence, models with similar μ_0/Q_T ratio show a linear dependence with the squared dipole, while the dipole fluctuations depend nontrivially on μ_0/Q_T and may upset the otherwise simple dependency on μ_0.

We are tempted to conclude that commonly employed rigid water models are unable to produce reliable dielectric constants for ice unless an artificial charge distribution is employed. Most likely, the results can only be improved by considering both polarizability and quantum effects. Some models incorporating polarizability provide fairly good dielectric constants for ice.[19] Furthermore, including quantum corrections to simple point charge models is known to soften the strength of interactions, changing the properties of the classical model to the equivalent of a shift of about 20−30 K.[57−59] As a result, a reparametrized model allows for a considerable increase of point charges to cope for the quantum effect,[58] and hence should also contribute to an increase of the dipole moment.

Anisotropy of the Dielectric Constant. Hexagonal crystals such as ice Ih are optically uniaxial, having one distinct direction parallel to the hexagonal axis and two equivalent directions chosen arbitrarily on the basal plane. Since the simulations are prepared in an orthorhombic arrangement with the z direction along the hexagonal axis, this implies that the dipole moment fluctuation tensor should become diagonal. The solution of eq 14 should yield two identical eigenvalues $\varepsilon_{xx} = \varepsilon_{yy} = \varepsilon_\perp$ corresponding to in plane fluctuations and one distinct eigenvalue $\varepsilon_{zz} = \varepsilon_\|$ corresponding to fluctuations along the hexagonal axis.

In practice, we found the anisotropy of the dielectric response very difficult to calculate. Already, we expect beforehand that the variance of individual components should be about 3 times larger than that of the dielectric tensor's trace. Not surprisingly, in our simulations, we find that the xx and yy components may differ among them as much as between the zz component, and there seems to be no systematic trend in that difference with temperature. We conclude that the anisotropy of the dielectric tensor of these models in ice Ih is small, and, at any rate, smaller than the statistical uncertainty of our results. These results are in line with the previous simulation results of Rick and Haymet;[19] i.e., the diagonal components exhibit some differences within a simulation but do not show a clear temperature trend.

TABLE 2: Dielectric Anisotropy of Ice V at $T = 180$ K and $p = 5000$ bar as Predicted by TIP4P/Ice[a]

run	ε_{xx}	ε_{yy}	ε_{zz}	$^1/_3Tr(\varepsilon)$
1	22	172	82	92
3	67	197	48	103
5	37	146	58	80
6	26	159	63	83
8	124	186	75	128
av	34(30)	164(16)	76(16)	94(13)
expt				157(4)

[a] Selection of five sets of results from an ensemble of 10 independent runs. The row labeled "av" gathers the average of the 10 sets, with the squared variance in parentheses. The last displays an interpolation from experimental results for metastable samples of polycrystaline ice V at $p \approx 6000$ bar.[62]

We note that Barkema and de Boer performed simulations for a related model on a lattice.[17] That model predicts in accordance with the TIP4P models a A/$Pna2_1$ low temperature phase, with a transition at a temperature of 36 K and a polarization factor at 273 K of about $G = 2.5$. In such models, the sampling is made easier by discretization and the authors found negligible anisotropy of the polarization factor.

It should be pointed out that the experimental situation is also not very clear. Kawada reported a significant anisotropy for ice, with the difference increasing at low temperature.[60] Other authors, however, have not observed any measurable differences down to 133 K.[2,61]

Although the anisotropy of ice Ih was difficult to calculate, other phases of ice do become highly anisotropic. In order to test the possibility of calculating dielectric anisotropies, we performed additional simulations of ice V using the TIP4P/Ice model. Ice V was chosen because it is the phase of ice with lower symmetry and should therefore facilitate the task. Ice V has monoclinic symmetry and is therefore an optically biaxial crystal, with three different dielectric constants, and one of the principal dielectric axes along the binary symmetry axis.

As with the case of ice Ih, off diagonal elements survive that are a few percent of the diagonal elements. We have checked that principal dielectric constants obtained by diagonalization of the dipole fluctuation tensor differ only by a few percent from the diagonal elements of the dipole fluctuation tensor obtained directly from the simulations. Within the error bars, the results obtained using eq 14 are equal to those obtained when the net dipole moment is assumed zero *a priori*. This gives us confidence in the reliability of our results. We should further note that, when using the standard Rahman−Parrinello NpT simulations, one must make sure that the dipole fluctuation tensor is collected from an orthogonal reference system that rotates together with the crystal. Otherwise, all information relevant to the anisotropy is washed away.

Table 2 collects a set of results obtained from 10 independent simulations of 4 million cycles each at 180 K and 5000 bar for

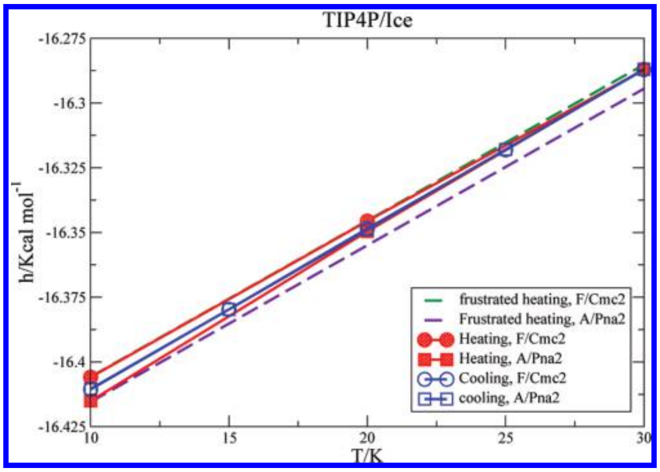

Figure 8. Enthalpy versus temperature isobars (P = 1 bar) close to absolute zero. Dashed lines correspond to frustrated heating batches starting from either A/$Pna2_1$ (violet) or F/$Cmc2_1$ (green) phases. Red hatched symbols correspond to heating batches starting from A/$Pna2_1$ (squares) and F/$Cmc2_1$ (circles). Blue empty symbols correspond to cooling batches starting from the high temperature branch of the corresponding heating batches.

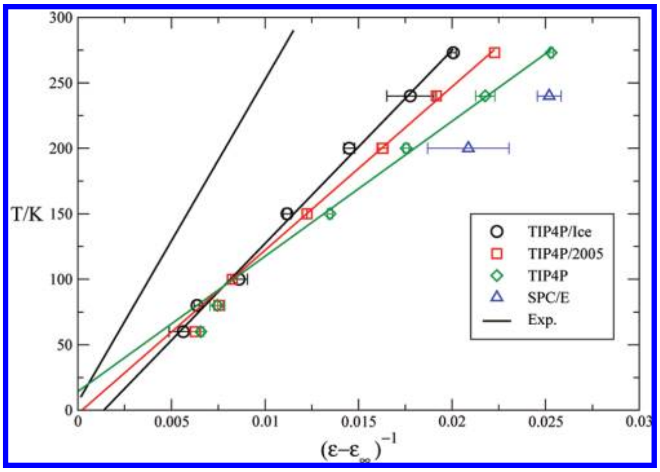

Figure 9. Curie−Weiss plot for several water models. The lines along the symbols are a linear fit of data from 273 to 150 K. For the rigid point charge models, $\varepsilon_\infty = 1$, while experimentally we assumed ε_∞ = 3.2 as in ref 2.

a system size of N = 224 molecules. Whereas a large scatter in the results is visible, we find clear indication of three distinct dielectric constants ε_{xx} = 43, ε_{yy} = 164, and ε_{zz} = 76, with related variance of 30, 16, and 16. The trace of the tensor yields ε = 94 and a smaller variance of 13. Comparing with the experimental result $\varepsilon \approx 157$ obtained for the same temperature and ≈6000 bar (ref 62) suggests again that the simulation result is far too small. Adopting the standard representation of ice V in the space group $C2/c$, with the binary axis along **b**, the principal dielectric axes may be chosen such that two lie along the **b** and **c** crystallographic axes, with the third one making an angle of about 20° with **a**.

Although we are able to resolve the anisotropy in this case, we should note that the results gathered here require 20 days of simulation on 10 processors at 2.4 MHz. This shows explicitly the difficulty of calculating dielectric anisotropies.

Order/Disorder Transition. Together with the results for the heating batches, Figure 4 shows the order parameters obtained during a cooling batch from the disordered high temperature phase. Clearly, the system remains fully disordered all the way from 100 to 5 K, since both O_F and O_A remain essentially equal to 0. This finding is consistent with two hypotheses. The first one is that the algorithm works well but the disordered phase is more stable than either the F/$Cmc2_1$ or A/$Pna2_1$ crystallographic structures. Note that, according to the third law, this would imply that there must be some other more stable low temperature phase for these models. The second one is that one of these two phases is the low temperature phase, but the order/disorder transition is irreversible due to poor sampling (this being the situation for actual hexagonal ice). In order to explore this issue further, we have calculated the enthalpy of F/$Cmc2_1$ and A/$Pna2_1$ and disordered phases down to very low temperatures. At constant pressure, the enthalpy provides the thermodynamic stability criteria as absolute zero is approached, so this test should allow us to find the most stable of all three phases.

Figure 8 shows the molar enthalpy as a function of temperature for TIP4P/Ice in the vicinity of absolute zero. The results are bracketed from below by A/$Pna2_1$ and from above by F/$Cmc2_1$. The equation of state for the ordered phases was obtained with a frustrated heating batch, with loop moves switched off. The results also include heating batches starting from either F/$Cmc2_1$ or A/$Pna2_1$, with loop moves on. The equation of state then follows the results for the corresponding frustrated batches, gradually departing and converging to a high temperature phase just below the results for the frustrated F/$Cmc2_1$ branch. The results indicate that A/$Pna2_1$ is the most stable of the three phases considered at low temperature. Cooling batches starting from the high temperature phase down to 10 K are also shown and appear to lie between the results for A/$Pna2_1$ and F/$Cmc2_1$. Thus, for the TIP4P/Ice model, the relative stability is A/$Pna2_1$ > Ih > F/$Cmc2_1$. The enthalpy of A/$Pna2_1$ remains below that of the disordered phase up to 50 K, so that entropy is indeed responsible for the transition. The results on the relative stability of ordered and disordered phases of TIP4P and SPC/E models agree with calculations reported previously by Rick.[20]

The equation of state results show that the disordering of the low temperature phase occurs at very low temperature. Those results agree with findings by Rick for several water models.[20] Although the equation of state results described above are far more reliable, it is interesting to point out that the temperature behavior of the dielectric constants obtained is also consistent with such predictions. Figure 9 displays a plot of T against $1/(\varepsilon - \varepsilon_\infty)$. According to the Curie−Weiss law, such a plot should be linear, with an intercept on the Curie−Weiss temperature. The results show that such linear dependence indeed holds up to about 150 K, with intercepts on the temperature axis that are below 15 K.

Similar results are obtained for the other TIP4P-like models (not shown), with the enthalpy increasing in the order A/$Pna2_1$ < Ih < F/$Cmc2_1$. The qualitative behavior of SPC/E is again somewhat different, as our results suggest that both A/$Pna2_1$ and F/$Cmc2_1$ are more stable than Ih at low temperature, with A/$Pna2_1$ again somewhat more stable than F/$Cmc2_1$. These observations are consistent with energy minimization results obtained by Buch et al. for several rigid point charge models, which systematically predicted the A/$Pna2_1$ phase as more stable than F/Cmc2_1. For such rigid point charge models, it seems the energy is an almost linear function of the cis−trans dimer populations.[63,64] Buch et al. suggested that the only way this order can be inverted in simple empirical models is by including a polarization center displaced from the oxygen along the HOH bisector.[63] However, it has been show that rigid point charge models such as the NvdE model of Nada and van der Eerden[65] predict the F/$Cmc2_1$ phase as the minimum energy structure.[20]

Consistent with observations by Rick and Haymet, we note here that the results for the energy at low temperature show considerable system size dependence.[20] The results reported here refer to systems with size $N = 360$ and $R_c = 8.5$ Å. For smaller systems ($N = 128$), a smaller cutoff radius has to be employed and the effect is as strong as to change the relative stability of F/$Cmc2_1$ and A/$Pna2_1$. Moreover, for such systems, the algorithm is more effective and the transition does become reversible. Buch et al. also observed a considerable energy dependence on the cutoff distance some time ago.[63] Intriguingly, the system size dependence reported by Buch et al. and Rick does not affect ab initio density functional methods which suggest that calculations with about 12−16 molecules provide all of the information that is needed to predict accurately the ground state energy.[66,67] Be as it may, we have checked that this system size dependence does not affect the high temperature results for the dielectric constant.

Overall, the results indicate that all four models studied in this work point to the antiferroelectric A/$Pna2_1$ phase as most stable, with an entropy driven transition to ice Ih at very low temperature. Whereas this result is at odds with the accepted experimental situation, which favors the ferroelectric F/$Cmc2_1$ phase,[12,13] it seems clear that theoretical prediction of the transition is certainly a major challenge. As Figure 8 shows, the enthalpy differences between different phases amount to about 0.010 kcal/mol. Considering the role of polarization, quantum effects, molecular vibrations, etc., that have been completely ignored in this study, one can very well accept discrepancies with experiment of such a small amount.

Buch et al. suggest that this problem can only be remedied by somehow including polarization effects. They found that an empirical model with a single polarization center predicts greater stability of F/$Cmc2_1$. Also, ab initio calculations using the empirical BLYP functional predict the F/$Cmc2_1$ phase as the most stable phase and a phase transtion at about 98 K.[66,67] However, this result must at this point be considered with some care, since the BLYP functional predicts a melting point of ice Ih of 411 K (140 above the experimental value).[68] It is not obvious why a functional that predicts incorrectly the experimental melting point of ice Ih should be so accurate in the prediction of other much more subbtle phase transitions involving also ice Ih.

Conclusions

In this paper, we have calculated the dielectric constant of ice for several water models (TIP4P/Ice, TIP4P/2005, TIP4P, and SPC/E). Consistent with previous findings for the TIP4P and SPC/E models,[19,21] we find that also TIP4P/Ice and TIP4P/2005 highly underestimate the dielectric constant.

The results of this work show that the dielectric constants correlate with the dipole to quadrupole ratio but surprisingly not quite with the dipole moment. In order to fully understand this observation, one needs to consider separately the dependence of the dielectric constant on the dipole moment and the polarization factor.

The polarization factor of ice Ih is fairly similar for the entire TIP4P class of models, with $G \approx 2.5$. For the three models with a similar value of G, the dielectric constant varies smoothly with the dipole moment. The SPC/E model predicts very different angular correlations, with $G \approx 1.8$ only. These correlations seem to depend nontrivially on the dipole to quadrupole ratio, with all of the TIP4P models exhibiting very similar values of such a ratio. This large difference in G between the TIP4P and SPC/E models is somewhat compensated by the relatively large dipole moment of the latter.

We have attempted to calculate the anisotropy of the dielectric response in ice Ih. Our results show that this is a very difficult task that requires extremely lengthy simulations. We have been unable to identify any anisotropy for the TIP4P/Ice model, which was studied somewhat more extensively than the others. We believe the anisotropy of this model is below the statistical accuracy of our results for the diagonal elements of the dielectric tensor, which is about 10%. We have been able to identify a large anisotropy for ice V, however. For these optically biaxial crystals, the principal dielectric constants are 34, 164, and 76 at a temperature of 180 K and 5000 bar.

As noted previously for the TIP4P and SPC/E models,[20] the TIP4P/Ice and TIP4P/2005 models undergo an order/disorder transition at very low temperatures. All four models predict that the antiferroelectric $Pna2_1$ phase conjectured by Davidson and Morokuma[8] is of lower energy than the ferroelectric $Cmc2_1$ phase favored by experiments.[12,13] The TIP4P family actually predicts the ferroelectric phase to be of higher energy than samples with quenched disorder. In view of the large discrepancies of the dielectric constants for ordinary ice, these predictions might well be in error, however. Molecular polarization and quantum effects could play a significant role. This point remains to be studied, but accounts of all of these effects will certainly require a major computational effort.

Acknowledgment. We would like to acknowledge helpful discussions with R. Whitworth, J. L. Aragonés, and C. McBride. This work was supported by Ministerio de Educacion y Ciencia through project FIS2007-66079-C02-01 and by Comunidad Autonoma de Madrid throught project MODELICO-P2009/ESP-1691.

References and Notes

(1) Petrenko, V. F.; Whitworth, R. W. *Physics of Ice*; Oxford University Press: Oxford, U.K., 1999.
(2) Johari, G. P.; Whalley, E. *J. Chem. Phys.* **1981**, *75*, 1333.
(3) Giauque, W. F.; Stout, J. W. *J. Am. Chem. Soc.* **1936**, *58*, 1144.
(4) Pauling, L. *J. Am. Chem. Soc.* **1935**, *57*, 2680.
(5) Kawada, S. *J. Phys. Soc. Jpn.* **1972**, *32*, 1442.
(6) Tajima, Y.; Matsuo, T.; Suga, H. *Nature* **1982**, *299*, 810.
(7) Matsuo, T.; Tajima, Y.; Suga, H. *J. Phys. Chem. Solids* **1986**, *47*, 165.
(8) Davidson, E. R.; Morokuma, K. *J. Chem. Phys.* **1984**, *81*, 3741.
(9) Minagawa, I. *J. Phys. Soc. Jpn.* **1981**, *50*, 3669.
(10) Minagawa, I. *J. Phys. Soc. Jpn.* **1990**, *59*, 1676.
(11) Leadbetter, A. J.; Ward, R. C.; Clark, J. W.; Tucker, P. A.; Matsuo, T.; Suga, H. *J. Chem. Phys.* **1985**, *82*, 424.
(12) Howe, R.; Whitworth, R. W. *J. Chem. Phys.* **1989**, *90*, 4450.
(13) Line, C. M. B.; Whitworth, R. W. *J. Chem. Phys.* **1996**, *104*, 10008.
(14) Jackson, S. M.; Nield, V. M.; Whitworth, R. W.; Oguro, M.; Wilson, C. C. *J. Phys. Chem. B* **1997**, *101*, 6142.
(15) Sanz, E.; Vega, C.; Abascal, J. L. F.; MacDowell, L. G. *Phys. Rev. Lett.* **2004**, *92*, 255701.
(16) Rahman, A.; Stillinger, F. H. *J. Chem. Phys.* **1971**, *55*, 3336.
(17) Barkema, G. T.; de Boer, J. *J. Chem. Phys.* **1993**, *99*, 2059.
(18) Barkema, G. T.; Newman, M. E. J. *Phys. Rev. E* **1998**, *57*, 1155.
(19) Rick, S. W.; Haymet, A. D. J. *J. Chem. Phys.* **2003**, *118*, 9291.
(20) Rick, S. W. *J. Chem. Phys.* **2005**, *122*, 094504.
(21) Lindberg, G. E.; Wang, F. *J. Phys. Chem. B* **2008**, *112*, 6436.
(22) Berg, B. A.; Muguruma, C.; Okamoto, Y. *Phys. Rev. B* **2007**, *75*, 092202.
(23) Berg, B. A.; Yang, W. *J. Chem. Phys.* **2007**, *127*, 224502.
(24) Londono, J. D.; Kuhs, W. F.; Finney, J. L. *J. Chem. Phys.* **1993**, *98*, 4878.
(25) Lobban, C.; Finney, J. L.; Kuhs, W. F. *J. Chem. Phys.* **2000**, *112*, 7169.
(26) MacDowell, L. G.; Sanz, E.; Vega, C.; Abascal, J. L. F. *J. Chem. Phys.* **2004**, *121*, 10145.

(27) Jorgensen, W. L.; Chandrasekhar, J.; Madura, J. D.; Impey, R. W.; Klein, M. L. *J. Phys. Chem.* **1983**, *79*, 926.

(28) Berendsen, H. J. C.; Grigera, J. R.; Straatsma, T. P. *J. Phys. Chem.* **1987**, *91*, 6269.

(29) Abascal, J. L. F.; Sanz, E.; Fernandez, R. G.; Vega, C. *J. Chem. Phys.* **2005**, *122*, 234511.

(30) Abascal, J. L. F.; Vega, C. *J. Chem. Phys.* **2005**, *123*, 234505.

(31) Docherty, H.; Galindo, A.; Vega, C.; Sanz, E. *J. Phys. Chem. B* **2007**, *111*, 8993.

(32) Monreal, I. A.; Cwiklik, L.; Jagoda-Cwiklik, B.; Devlin, J. P. *J. Phys. Chem. Lett.* **2010**, *1*, 290.

(33) Rick, S. W.; Freeman, D. L. *J. Chem. Phys.* **2010**, *132*, 054509.

(34) Hill, N. E. *Dielectric properties and molecular behavior*; Van Nostrand Reinhold Co.: London, 1969.

(35) Kirkwood, J. G. *J. Chem. Phys.* **1939**, *7*, 911.

(36) Fröhlich, H. *Trans. Faraday Soc.* **1948**, *44*, 238.

(37) de Leeuw, S. W.; Perram, J. W.; Smith, E. R. *Proc. R. Soc. London, Ser. A* **1980**, *373*, 27.

(38) Neumann, M. *Mol. Phys.* **1983**, *50*, 841.

(39) Neumann, M.; Steinhauser, O.; Pawley, G. S. *Mol. Phys.* **1984**, *52*, 97.

(40) Allen, M.; Tildesley, D. *Computer Simulation of Liquids*; Clarendon Press: Oxford, U.K., 1987.

(41) Frenkel, D.; Smit, B. *Understanding Molecular Simulation*, 2nd ed.; Academic Press: San Diego, CA, 2002.

(42) Powles, J. G. *Trans. Faraday Soc.* **1955**, *51*, 377.

(43) Kusalik, P. G.; Mandy, M. E.; Svishchev, I. M. *J. Chem. Phys.* **1994**, *100*, 7654.

(44) Garzon, B.; Lago, S.; Vega, C. *Chem. Phys. Lett.* **1994**, *231*, 366.

(45) Born, M.; Wolf, E. *Principles of optics: electromagnetic theory of propagation, interference and diffraction of light*, 5th ed.; Pergamon Press: Oxford, U.K., 1975.

(46) Parrinello, M.; Rahman, A. *J. Appl. Phys.* **1981**, *52*, 7182.

(47) MacDowell, L. G. Ph.D. thesis, Universidad Complutense de Madrid, 2000.

(48) Rahman, A.; Stillinger, F. H. *J. Chem. Phys.* **1972**, *57*, 4009.

(49) Vega, C.; Abascal, J. L. F.; Sanz, E.; MacDowell, L. G.; McBride, C. *J. Phys.: Condens. Matter* **2005**, *17*, S3283.

(50) McBride, C.; Vega, C.; Sanz, E.; MacDowell, L. G.; Abascal, J. L. F. *Mol. Phys.* **2005**, *103*, 1.

(51) Adams, D. J. *Nature* **1981**, *293*, 447.

(52) Batista, E. R.; Xantheas, S. S.; Jonsson, H. *J. Chem. Phys.* **1998**, *109*, 4546.

(53) Sharma, M.; Resta, R.; Car, R. *Phys. Rev. Lett.* **2007**, *98*, 247401.

(54) Abascal, J. L. F.; Vega, C. *J. Phys. Chem. C* **2007**, *111*, 15811.

(55) Abascal, J. L. F.; Vega, C. *Phys. Rev. Lett.* **2007**, *98*, 237801.

(56) Rick, S. W. *J. Chem. Phys.* **2005**, *120*, 6085.

(57) de la Peña, L. H.; Kusalik, P. G. *J. Chem. Phys.* **2004**, *121*, 5992.

(58) McBride, C.; Vega, C.; Noya, E. G.; Ramirez, R.; Sese, L. *J. Chem. Phys.* **2009**, *131*, 024506.

(59) Noya, E. G.; Vega, C.; Sese, L.; Ramirez, R. *J. Chem. Phys.* **2009**, *131*, 124518.

(60) Kawada, S. *J. Phys. Soc. Jpn.* **1978**, *44*, 1881.

(61) Wörz, O.; Cole, R. H. *J. Chem. Phys.* **1969**, *51*, 1546.

(62) Johari, G. P.; Whalley, E. *J. Chem. Phys.* **2001**, *115*, 3274.

(63) Buch, V.; Sandler, P.; Sadlej, J. *J. Phys. Chem. B* **1998**, *102*, 8641.

(64) Bartok, A.; Baranyai, A. *J. Non-Cryst. Solids* **2007**, *353*, 2698.

(65) Nada, H.; van der Eerden, J. P. *J. Chem. Phys.* **2003**, *118*, 7401.

(66) Singer, S. J.; Kuo, J.-L.; Hirsch, T. K.; Knight, C.; Ojamäe, L.; Klein, M. L. *Phys. Rev. Lett.* **2005**, *94*, 135701.

(67) Knight, C.; Singer, S. J.; Kuo, J.-L.; Hirsch, T. K.; Ojamäe, L.; Klein, M. L. *Phys. Rev. E* **2006**, *73*, 056113.

(68) Yoo, S.; Zen, X. C.; Xantheas, S. S. *J. Chem. Phys.* **2009**, *130*, 221102.

JP100167Y